Tetrahedral framework nucleic acids-based delivery of microRNA-155 inhibits choroidal neovascularization by regulating the polarization of macrophages

Xin Qin [a,1], Lirong Xiao [b,1], Ni Li [b], Chen Hou [b], Wenman Li [b], Jiajie Li [a], Naihong Yan [b,**], Yunfeng Lin [a,c,*]

[a] State Key Laboratory of Oral Diseases, National Clinical Research Center for Oral Diseases, West China Hospital of Stomatology, Sichuan University, Chengdu, 610041, China
[b] Research Laboratory of Ophthalmology, West China Hospital, Sichuan University, Chengdu, 610041, China
[c] College of Biomedical Engineering, Sichuan University, Chengdu, 610041, China

ABSTRACT

Choroidal neovascularization (CNV) is a common pathological feature of various eye diseases and an important cause of visual impairment in middle-aged and elderly patients. In previous studies, tetrahedral framework nucleic acids (tFNAs) showed good carrier performance. In this experiment, we developed microRNA-155-equipped tFNAs (T-155) and explored its biological effects on CNV. Based on the results of in-vitro experiments, T-155 could regulate macrophages into the antiangiogenic M1 type. Then, we injected T-155 into the vitreous of laser-induced CNV model mice and found that T-155 significantly reduced the size and area of CNV, inhibited blood vessel leakage. In summary, we prove that T-155 could regulate the inflammatory process of CNV by polarizing macrophages, thereby improving the symptoms of CNV. Thus, T-155 might become a new DNA-based drug with great potential for treating CNV.

1. Introduction

Age-related macular degeneration (AMD) is one of the main causes of blindness, and it mainly occurs in people (> 60 years old) of developed countries. With the aging of the population in many countries, approximately 196 million patients will suffer from age-related macular degeneration in 2020, and the number will increase to 288 million in 2040 [1,2]. The main feature of advanced wet AMD is choroidal neovascularization (CNV), which is accompanied by a series of serious adverse reactions, such as sub-retinal hemorrhage, photoreceptor damage, and severe central visual impairment [3,4].

Although the pathogenesis of CNV has not yet been fully elucidated, immune-vascularization interactions are closely related to CNV [5,6]. CNV is a chronic inflammation-related degenerative disease, and its main feature is the proliferation of blood vessels in the fundus. In human neovascular age-related macular degeneration (NVAMD), histopathology of CNV frequently reveals the presence of macrophages, and macrophage frequency is increased in thicker, more fibrotic lesions. In the murine laser-induced CNV model, it have similarly observed that macrophages infiltrate CNV lesions. The murine laser-induced CNV model can reflect the classic CNV patients and assess CNV development as part of a wound healing response to more extensive injury [7–9]. It is generally known that there are two sources of macrophages in the CNV model, one is microglia that migrates from the retina to the CNV lesion, and the other is blood-derived macrophages that migrate from the circulation. Since microglia are tissue resident macrophages at steady state and unaffected by laser injury, research shows that blood-derived macrophages are the more important source and more related to the pathological process of CNV [10,11].

The strong plasticity of macrophages is its main characteristic [12].

Macrophages are polarized into a classic activation type (M1) that resists angiogenesis and a repair type (M2) that promotes angiogenesis. M1 and M2 macrophages express different characteristic chemokines that determine their different roles. M1-type macrophages mainly increase the levels of nitric oxide synthase, interleukin-1β (IL-1β), IL-12, CCL-3, and CCL-5, which are mainly activated by bacterial lipopolysaccharides and interferon-γ. While M2-type macrophages mainly present increased levels of arginase-1 (Arg-1), resisting-like-α (Fizz-1), chitinase 3-like 3 (Ym-1), CD206, and CD163, which are induced by IL-4, IL-10 or PGE2 [13–15]. M0/M1/M2 type macrophages exist in different proportions in different microenvironments in vivo, maintaining a delicate balance. In the in vivo environment, the M1/M2 paradigm is not completely similar to in vivo. The increase of M1 macrophages does not necessarily cause inflammation. However, studies have shown that CNV pathobiology generally accepts the concept that M2 macrophages mediate the formation and growth of CNV [9]. In the CNV microenvironment, although it has not been fully understood, a chronic inflammatory response has always existed [16,17]. This inflammatory response will affect the differentiation of various phenotypes of macrophages, and then change the proportion of each cell secretion (such as VEGF, TNF-α, IL-8, etc., which are closely related to angiogenesis). These changes break the original balance, which in turn affects the microenvironment of inflammation [7, 18]. So we think that if we can improve this balance, maybe we can further improve the symptoms of CNV.

However, in clinical treatment, the direct regulatory factor for angiogenesis, vascular endothelial growth factor (VEGF), has occupied the main role [19,20]. VEGF inhibitors, such as bevacizumab and ranibizumab, are widely used. However, many problems remain. Many patients suffer from incomplete response to anti-VEGF therapy, which is defined as persistent (plasma) fluid exudation; unresolved or new hemorrhage; progressive lesion fibrosis; suboptimal vision recovery. Incomplete response to anti-VEGF therapy is the bottleneck of treatment [9]. From a practical perspective, long-term repeated intravitreal injections of these drugs impose substantial burdens on patients' psychological and economic conditions. Thus, the novel treatments for CNV need to be developed [21,22].

In the experimental CNV model, a large number of macrophages infiltrate the lesion site in the early stage after laser injury. Based on these findings, the presence of macrophages and the proportion of the two polarized phenotypes may affect the occurrence and development of CNV lesions. Therefore, methods with the ability of effective and accurate regulation of the macrophage polarization are needed, which could inhibit the process of CNV. Using the macrophages as supplement or target may broaden the landscape and paradigms for NVAMD treatment.

In terms of drug or gene delivery, tetrahedral framework nucleic acids (tFNAs) are a promising vector. The tFNAs are a three-dimensional structure synthesized from four pieces of single strand DNA [23–25]. Due to the source of its components, its good biosafety and biocompatibility have been proven in previous studies [26–28]. In addition, accumulating evidence shows that tFNAs quickly penetrate cells and enter mammalian cells through pore-mediated endocytosis due to their special three-dimensional structure and remain intact for up to 48 h [29–31]. At the same time, tFNAs escape from lysosomes through nuclear localization signals, which ensure their stability and efficiency in the process of gene delivery [32,33]. For the stable structure and special properties of tFNAs, the vector has been proven to carry some small-molecule drugs, peptide fragments, and RNA fragments into the cell with extremely high efficiency [34–38].

MicroRNAs (miRNAs) are noncoding RNAs that regulate the protein expression of target genes by pairing with target mRNA sequences [39]. An increasing number of studies have proven that miRNAs extensively regulate biological processes, and certain miRNAs are also involved in the polarization of macrophages. MicroRNA155 (miRNA-155) is very active in the immune process [40,41]. The expression of miRNA-155 is increased in various activated immune cells, which is very sensitive to inflammation. Relevant studies have shown that changes in

microRNA-155 expression are related to the formation of new blood vessels [42,43]. In a mouse laser-induced CNV model, miRNA-155 is downregulated from day 1 to day 3 and upregulated on day 14. Thus, miRNA-155 is a potential therapeutic target, and early and timely upregulation of miRNA-155 may exert therapeutic effects [44]. Zhang et al. [43] found miR-155 inhibits polarization of macrophages to M2-Type and suppresses CNV. Over-expression of miR-155 inhibited M2 polarization through targeting C/EBPβ, suppressed VEGF expression and the formation of CNV after injury. And miR-155 is key to M2 macrophages in CNV micro-environment. In this experiment, we used tFNAs carrying miRNA-155 (T-155) to polarize macrophages and observed the effects of polarized macrophages on CNV model mice. Our experiments have proven that tFNAs with miRNA-155 efficiently polarizes macrophages to the M1 type and significantly reduces fundus leakage and angiogenesis in CNV mice. This study provides a new treatment strategy for CNV-related diseases and NVAMD. In addition, due to the unique structure of tFNAs, we can connect more targeted drugs or sustained-release systems to the rest apex of T-155 in the future to achieve better therapeutic effects.

2. Materials and methods

2.1. Materials

Four ssDNA and microRNA-155 mimics were synthesized and characterized by Sangon (Shanghai, China). The Cell Counting Kit (CCK-8) was purchased from Shanghai Dojindo Technology Chemical Corp. The fluorescent 2′,7′-dichlorofluorescein diacetate (DCFH-DA) Kit was purchased from Beyotime (Shanghai, China). ProteoPrep® Total Extraction Sample Kits were purchased from Keygen (Jiangsu, China). All antibodies used for protein determination were purchased from Abcam (Cambridge, U.K.).

2.2. Synthesis of tFNA and T-155

First, TM buffer with a pH of 8.0 containing 10 mM Tris-HCl and 50 mM MgCl2 was prepared. Then, equal concentrations of the four ssDNAs were poured into TM buffer. After thorough mixing and centrifugation, the mixed solution was heated to 95 °C for 10 min and then cooled to 4 °C for 20 min to obtain tFNAs.

The synthesized tFNAs were added to modified microRNA-155 mimics at equal concentrations and incubated for 30 min at room temperature to obtain T-155. The base sequence of microRNA-155 mimics were listed in Table 1, and the mimics are purchased from Sangon (Shanghai, China), like the four ssDNAs.

The sequences of the four ssDNAs and modified miRNA-155 mimics are shown in Table 1.

2.3. Characterization of tFNA and T-155

We conducted experiments using the methods described in previous studies to verify the successful synthesis of tFNA and T-155 [45]. Briefly, we used PAGE and high-performance capillary electrophoresis (HPCE) to detect the difference in the molecular weights of tFNA and T-155 and then used a nanoparticle size analyzer to detect the difference between the zeta potential and particle sizes of the two reagents to determine whether the synthesis was successful.

2.4. Cell culture

Mouse macrophage cells (RAW264.7) and human umbilical vein endothelial cells (HUVECs) were both purchased from ATCC. We cultivated the cells with Dulbecco's modified Eagle's medium supplemented with 10% fetal bovine serum, 1 g/L glucose, and 1% antibiotic solution (100 U/mL penicillin and 100 μg/mL streptomycin) in an atmosphere comprising 95% air and 5% CO2 at 37 °C according to the

Table 1
The sequences of the four ssDNAs (The sequence of sticky ends is marked in bold).

ssDNA	Base sequence (5′-3')
S1	ATTTATCACCCGCCATAGTAGACGTATCACCAGGCAGTTGAGACGAACATTCCTAAGTCTGAA
S2	ACATGCGAGGGTCCAATACCGACGATTACAGCTTGCTACACGATTCAGACTTAGGAATGTTCG
S3	**TTGACCTGTGAATT**ACTACTATGGCGGGTGATAAAACGTGTAGCAAGCTGTAATCGACGGGAAGAGCATGCCCATCC
S4	ACGGTATTGGACCCTCGCATGACTCAACTGCCTGGTGATACGAGGATGGGCATGCTCTTCCCG
microRNA-155mimic sense	**UUCACAGGUCAA**UUAAUGCUAAUUGUGAUAGGGGU
microRNA-155mimic antisense (5′-3')	CCCUAUCACAAUUAGCAUUAAUU

manufacturer's instructions.

2.5. Uptake of Cy5-loaded-tFNA-155

Previous studies have successfully shown that tFNAs successfully enters RAW264.7 cells [46]. In this experiment, we tested whether tFNAs155 equipped with miRNA-155 successfully entered cells. We modified one of the ssDNAs in the tFNAs into ssDNA labeled with Cy5 fluorescence, added the modified T-155 to RAW264.7 cells, measured the fluorescence intensity at several time points (6 h and 14 h) and compared it with the blank control group. In simple terms, the experimental operation was to digest and harvest the cells, wash them three times with phosphate-buffered saline, and use flow cytometry to detect the fluorescence intensity.

2.6. Assessment of cell viability

We plated RAW264.7 cells in a 96-well plate at a density of 6000 cells per well to detect drug toxicity. Then, the cells were divided into four groups, a blank group and groups treated added with equal concentrations of tFNAs miRNA-155mimics, or T155. The medium was aspirated after 24 h, and cells were washed with PBS three times before 10 μL of the CCK-8 solution were added to each well. After 2 h of incubation, the 96-well plate was placed in a microplate reader and the absorbance was detected at 450 nm.

2.7. Quantitative PCR

We used quantitative PCR (Q-PCR) technology to detect the expression of related genes in M1 macrophages and the target genes of microRNA-155. After extracted the total RNA from the cells, the PrimeScript RT reagent Kit (TaKaRa, Dalian, China) was used to transcribe the RNA into cDNAs. Then, the PrimeScript RT-PCR Kit (TaKaRa, Dalian, China) and primers for the relevant genes (C/EBPβ, CD40, VEGF, and iNOS) were used to complete the PCR amplification process using the method described in a previous study. The sequences of PCR primers are listed in Table 2.

2.8. Immunofluorescence staining

We used an ultrahigh-resolution two-photon laser confocal microscope to observe the morphology and the expression of related proteins.

Table 2
The sequences of PCR primers.

mRNA	Primer pair (5′-3')
VEGF	Forward TAGAGTACATCTTCAAGCCGTC
	Reverse CTTTCTTTGGTCTGCATTCACA
CD40	Forward AGCGGTCCATCTAGGGCAGTG
	Reverse GTGGCTTGTCAGTCGGCTTCC
C/EBPβ	Forward TCTCTGCTTCTCCCTCTGCC
	Reverse ACAGCAACAAGCCCGTAGG
iNOS	Forward TGGTCCGCTAGAGAGTGCT
	Reverse CCTCATTGGCCAGCTGCTT

The cells were seeded in advance in a 12-well plate containing coverslips and grouped and processed using the method described above. Then, the cells were washed three times, fixed with 4% paraformaldehyde and permeabilized with 0.5% Triton X-100. Goat serum was used to seal the pores of the cells and prevent false positives, and then the corresponding antibodies were added and incubated overnight. Afterwards, a fluorescent secondary antibody was incubated with the cells, and DAPI and phalloidin were used to stain the nucleus and cytoskeleton, respectively.

2.9. Angiogenesis experiment

We processed the macrophages in groups using the aforementioned method,[28,30] harvested these cells and plated them in the upper transwell chamber to test whether drug-treated macrophages inhibit the formation of new blood vessels. The well below the transwell chamber was preplated with human umbilical vein endothelial cells at the same density. After the two cell types were cocultured for 24 h, the HUVECs were harvested separately and replated in 96-well plates precoated with Matrigel (Corning, Hefei, China). After 4 h of incubation in the incubator, the vascularization of HUVECs was observed under a microscope, photographed, and analyzed.

2.10. Laser-induced CNV model

C57BL/6J mice (6–8 weeks, male) were purchased from the Animal Experiment Center of Sichuan University. These mice were anesthetized with 1% pentobarbital sodium (50 mg/kg) after dilating the pupils with tropicamide. Laser photocoagulation (laser spot diameter-50 μm, duration-100 ms, 270 mW, 4–6 spots/eye) was performed using an ophthalmic laser photocoagulation apparatus (532-nm Laser, MD-960, MEDA Co., Ltd., Tianjin, China) under a slit lamp microscope (YZ5F, Suzhou 66 Vision Technology Co. Ltd., Jiangsu, China). The laser spots were approximately 2.5-3-disc diameters from the head of the optic nerve, avoiding the main blood vessel. A white bubble formed at each point, indicating Bruch's membrane rupture that subsequently leads to CNV.

2.11. Intravitreal injection

Five days after laser treatment, 2 μL of T-155 (the concentration is 1000 nM)were injected into the vitreous cavity, and an equivalent volume of PBS/tFNAs/155mimics was used as the control group. First, the mice were anesthetized with 1% pentobarbital sodium (50 mg/kg). Next, a small hole was generated with a 30-gauge needle near the limbus, and then a blunt 31-gauge needle (Hamilton syringe) was inserted into the vitreous cavity through the hole. Antibiotics were applied to the conjunctival sac of each animal.

2.12. Fundus fluorescence angiography (FFA)

On the 8th day of laser photocoagulation, CNV was assessed in the mice using FFA. The instrument was a Spectralis HRA ophthalmic diagnostic apparatus (Heidelberg, Germany). Briefly, mice were anesthetized with 1% pentobarbital sodium (50 mg/kg) after dilating the

pupils. FFA images were captured at appropriate intervals after an intraperitoneal injection of 200 μL of 2% fluorescein sodium. The FFA images captured at the same time point were analyzed by ImageJ software. Areas and intensity were measured.

2.13. Choroidal flat mounts

Eight days after the laser treatment, eyes were fixed with 4% PFA for 40 min, and the cornea, crystalline lens and retina were removed from each eye. The remaining eyecup tissues were incubated with FITC-conjugated isolectin-B4 (IB4; L2895) at 4 °C for 48 h. After repeated washes with 1 × PBS, the tissues were cut into a clover shape and mounted onto glass slides. Images were captured with a fluorescence microscope. The IB4-positive CNV regions were quantified with ImageJ software.

2.14. Histopathology

The eyes were removed 8 days after laser treatment, soaked in a 10% buffered formalin solution, embedded in paraffin, sliced (5 μm thickness), and stained with hematoxylin and eosin. Images were obtained with an optical microscope, and ImageJ software was used to quantify the CNV lesions.

2.15. Statistical analysis

All data are presented as the means ± standard deviations (SD). The ANOVA test was applied to detect significant differences between test group and another group. When $p < 0.05$, differences were regarded as statistically significant.

3. Results and discussion

3.1. Characterization of the tFNAs and T-155

Fig. 1 briefly shows the synthesis process of T-155 and the process by

which polarized macrophages reduce CNV symptoms.

Four single-stranded DNAs (Table 2) were successfully synthesized into tFNAs. A brief description of the synthesis of tFNAs and T-155 is provided in Fig. 2A. Among the ssDNAs, the unique sticky end designed on the S3 chain is complementary to the sticky end derived from microRNA-155. After processing, a vertex of tFNAs is connected to microRNA-155 to become T-155. The results of polyacrylamide gel electrophoresis (PAGE) showed a large difference the molecular weights of the four ssDNAs and the synthesized tFNAs. Notably, the molecular weight of T-155 was greater than the molecular weight of tFNAs, indicating that microRNA-155 was successfully connected to tFNAs (Fig. 2B) [47]. At the same time, capillary electrophoresis was also used to detect the successful synthesis of tFNAs, and the data were consistent with the PAGE results (Fig. 2C and Fig. S1 in supplementary data). We used dynamic light scattering (DLS) to detect some related properties of tFNAs and T-155 and further confirm the successful synthesis of tFNAs. The zeta potentials and particle sizes of tFNAs and T-155 were near the theoretical values, namely, they were both negatively charged and had a particle size less than 20 nm (Fig. 2D and E, and Fig. S3 in supplementary data) [48].

3.2. Cellular uptake of T-155

In previous studies, tFNAs were shown to successfully and quickly enter RAW264.7 cells [46]. Therefore, we verified whether T-155 equipped with miRNA-155 could successfully enter RAW264.7 cells. We replaced one of the ssRNAs of T-155 with a ssDNA labeled with Cy5 fluorescence, added the complex to the cell culture medium, harvested the cells at different time points and used flow cytometry to detect the proportion of fluorescent cells to determine the uptake of T-155. As shown in Fig. 2F and supplementary data Fig. S3, the proportion of fluorescent cells gradually increased over time and reached more than 90% at 14 h. Based on this result, T-155 relies on the unique structure of tFNAs to successfully enter cells, laying the foundation for the effect of miRNA-155.
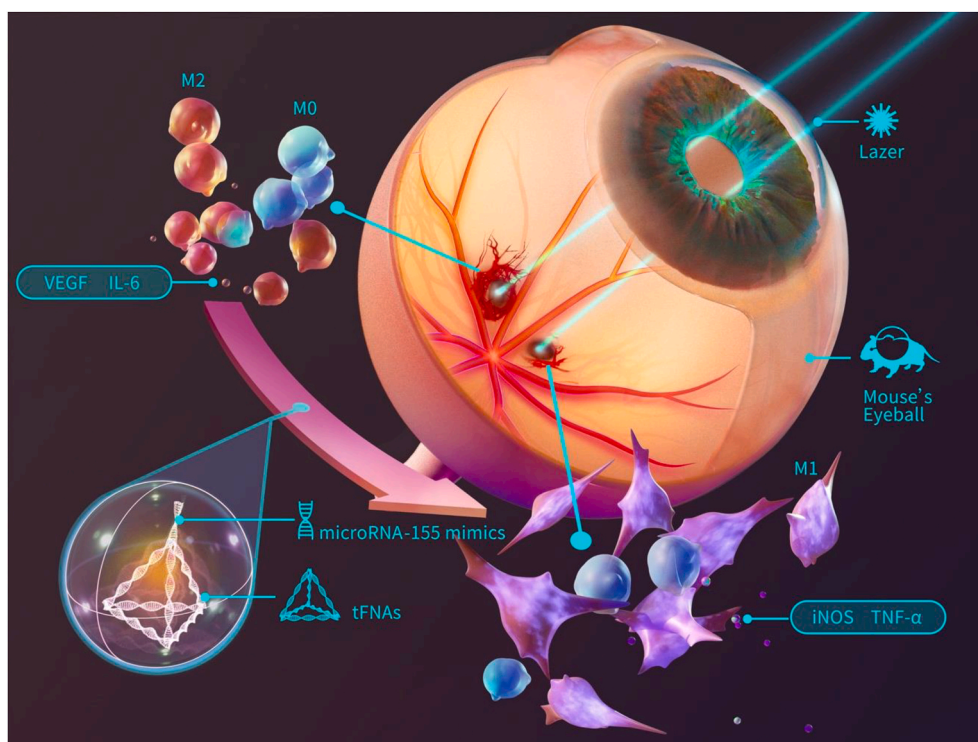

Fig. 1. Graphic abstract. The synthesis process of T-155 and the process by which polarized macrophages reduce CNV symptoms.
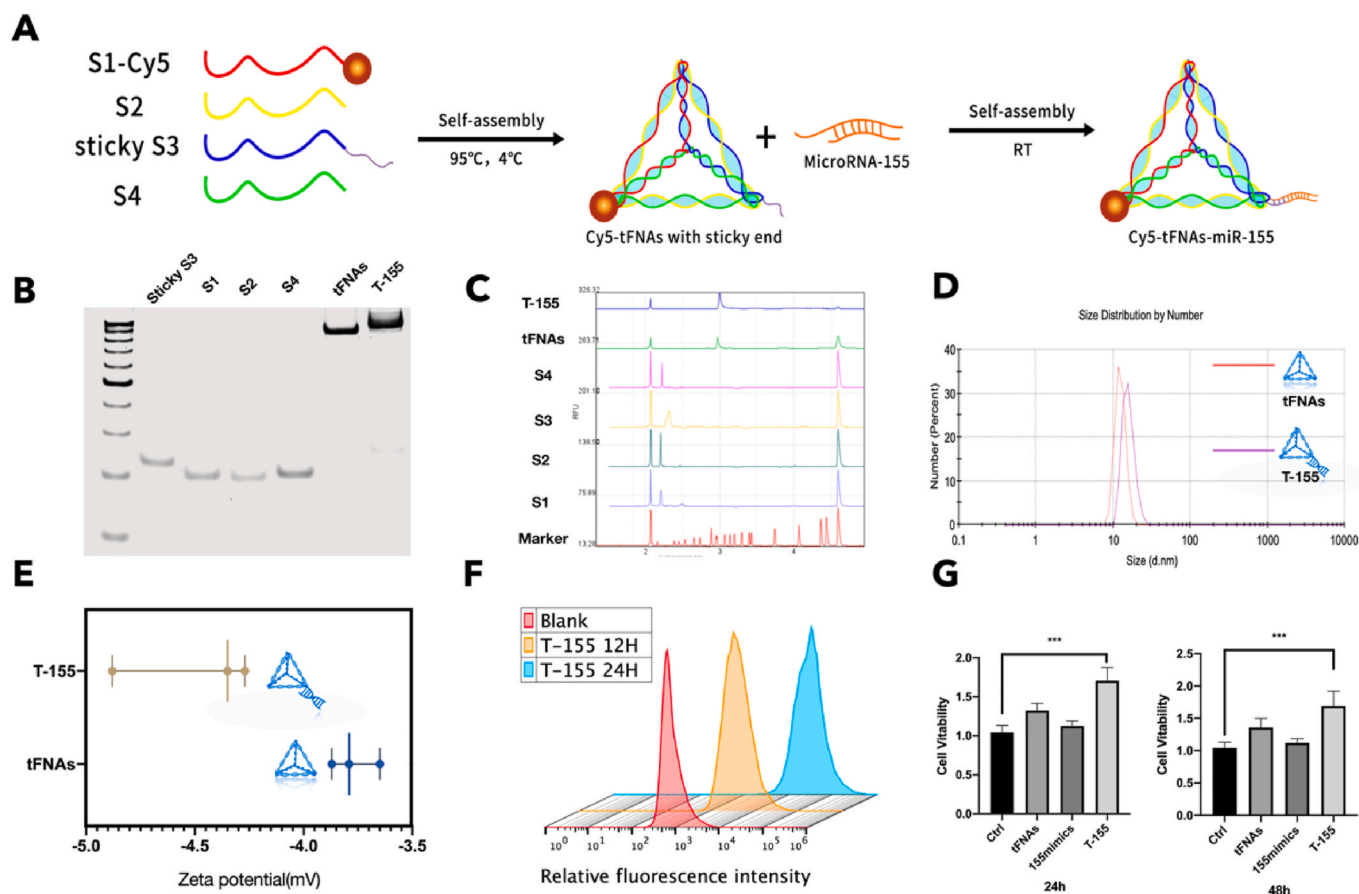
Fig. 2. Characterization of tFNAs and T-155. (A) A brief description of the synthesis of tFNAs and T-155. (B) The results of polyacrylamide gel electrophoresis (PAGE). (C) The results of capillary electrophoresis. (D) Particle sizes of tFNAs and T-155 (E) Zeta potentials of tFNAs and T-155. (F) Cellular uptake of T-155 in three different time point. (G) The cytotoxicity test of T-155. (n = 6) Statistical analysis: the ANOVA test was applied, ***p < 0.001 and ****p < 0.0001.

3.3. Cytotoxicity of tFNAs and T-155

Compared with other RNA transfection reagents, tFNAs stand out because of their good biosafety and biocompatibility. According to previous studies, tFNAs are nontoxic to cells and effectively promote the proliferation, migration and differentiation of certain cells [47,49–52]. In this experiment, we tested the cytotoxicity of tFNAs and T-155 towards RAW264.7 cells. Briefly, we cultured tFNAs and T-155 at a concentration of 250 nm with RAW264.7 cells for 24 h and 48 h, and then used the CCK-8 kit to detect cell viability. At the same time, we also conducted experiments with microRNA155 mimics as a control group to observe whether microRNA-155 mimics can function without any carrier assistance. As shown in Fig. 2G, tFNAs promoted the proliferation of RAW264.7 cells compared to the control group, consistent with the results of previous studies. More specifically, T-155 equipped with microRNA-155 exerted a stronger effect on promoting the cell viability of RAW264.7 cells.

3.4. The effect of T-155 on the polarization state of macrophages

In our experiments, we found that T-155 could promote the polarization of macrophages to M1 type (Fig. 3A). We used PCR technology to detect the quantity of related genes and further determine whether the miRNA-155 mimics attached to the apexes of tFNAs could play a role after T-155 entering the cell. After miRNA-155 entering cells, it mainly acts by inhibiting C/EBPβ [42,53]. Therefore, we first detected the amount of this gene after transfection and observed significantly lower expression of C/EBPβ in the T-155 group than in the other groups. In addition, we also studied the expression levels of secreted factors in M1

and M2 macrophages. Lipopolysaccharide (LPS) is a typical M1 macrophage activator [12,14]. Here, we used LPS as a positive control to observe whether the changes in the levels of cytokines secreted by macrophages after T-155 treatment were consistent with the trend observed in the LPS group. As shown in Fig. 3F, higher levels of VEGF were secreted from M2-type macrophages, but the levels decreased after T-155 treatment. In contrast, the levels of iNOS and CD40, characteristic markers of M1-type cells, were increased. [12] This result is also consistent with the result obtained after LPS treatment.

After genetic verification, we performed immunofluorescence staining to detect changes at the protein level, and further confirm that the macrophages treated with T-155 were polarized towards the M1 phenotype. As mentioned above, we measured the levels of secreted factors specifically expressed in M1 macrophages (IL-1β, TNFα, and IL-6) IL-1β,TNFα and IL-6 levels increased in macrophages after T-155 treatment, consistent with the results from the LPS group (Fig. 3B–E). This finding also proved that RAW264.7 cells were polarized into M1-type cells after the T-155 treatment.

Finally, in addition to changes in the levels of secreted factors, the morphology of macrophages also changed after the T-155 treatment. Most of the untreated RAW264.7 cells were round in shape and displayed a three-dimensional morphology. A polymorphic shape was observed for RAW264.7 cells after T-155 treatment. In general, compared to the cells before treatment, most of the cells extended pseudopods, the shape was flattened, and the pseudopods became slenderer (supplementary data S4).

In summary, changes from genes to proteins to cell morphology have all proven that T-155 successfully induces macrophage polarization to the M1 type, laying the foundation for subsequent macrophages to exert
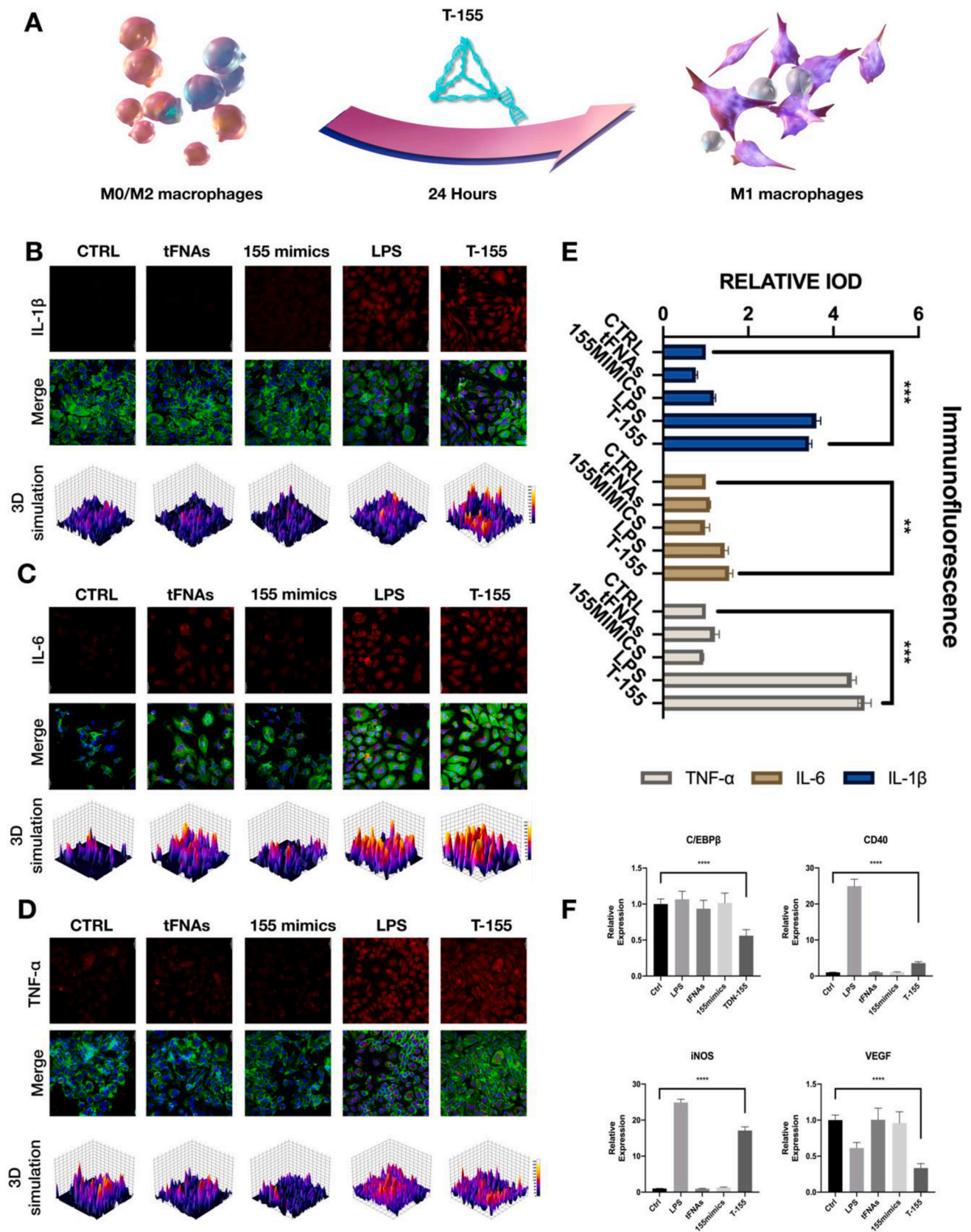
Fig. 3. T-155 can promote the polarization of macrophages to M1 type. (A) A brief description of T-155 promotes the M1-type polarization process of macrophages. (B) Immunofluorescence micrographs of IL-1β (cytoskeleton: green, nucleus: blue, IL-1β: red). Scale bars are 20 μm The same below. (C) Immunofluorescence micrographs of IL-6 (IL-6: red). (D) Immunofluorescence micrographs of TNF-α (TNF-α: red). (E) The relative protein expression intensity of the three proteins. Data are presented as mean ± SD (n = 3). (F) Relative gene expression of C/EBP β, CD40, iNOS and VEGF in macrophages after treatment in different group. Statistical analysis: the ANOVA test was applied, ***p < 0.001 and ****p < 0.0001. All images in Figure are representative images.

their antiangiogenic effects.

3.5. T-155-treated macrophages inhibit angiogenesis

Although previous experiments have proven that T-155 promoted the polarization of macrophages to M1-type macrophages, whether polarized macrophages could truly inhibit the formation of blood vessels remains to be further explored. Therefore, we used transwell chambers to coculture polarized macrophages and human umbilical vein endothelial cells (HUVECs) and to observe the angiogenesis of HUVECs after coculture.

After 24 h of cocultivation, as shown in Fig. 4A, no difference was observed between the control group, TFNAS group and miR-155mimic group. In contrast, blood vessel formation was significantly inhibited in the T-155 group, which was similar to the LPS group. Then, we used Image J software (version 1.53) to analyze blood vessel formation and the number of blood vessel networks, the length of blood vessels formed, and the number of blood vessel nodes (Fig. 4B). After T-155 treatment, when co-culturing macrophages with HUVECs, macrophages significantly inhibited the formation of the blood vessel lumen, inhibited the formation of blood vessel nodes and reduced the length of the blood vessels that formed. Macrophages cultured with T-155 exerted a substantial inhibitory effect on the formation of blood vessels, which laid the foundation for our subsequent in vivo experiments.

3.6. Intraocular injection of T-155 effectively inhibits CNV in mice after laser treatment

In order to further determine the therapeutic effect of T-155 on CNV in vivo, we used laser to establish a CNV model in mice. The specific process is briefly described in Fig. 4B. We used the method described above to construct a mouse CNV model and further confirm the effect of T-155 on CNV in vivo. On day 5, mice with successful fundus contrast screening indicating the establishment of CNV were injected intraocularly. After the second image was captured on day 8, the mice were sacrificed to harvest samples [54].

Angiogenesis is a physiological process of tissue growth and repair that is regulated by factors that both promote and inhibit angiogenesis. In the establishment of CNV animal models induced by laser photocoagulation, the thermal effect, mechanical damage effect and photochemical effect of lasers can be used to selectively destroy the retinal pigment epithelium(RPE)-Bruch membrane-choroid capillary complex, activate the damage repair process, and disrupt the balance between angiogenic factors and inhibitors, which induces angiogenesis [55–58]. A new blood vessel is only a tube surrounded by simple endothelial cells. It lacks surrounding connective tissue, a basement membrane, and receptors to sense blood flow or blood pressure. Due to the incomplete development of the tube wall, these blood vessels are fragile and are prone to rupture and bleeding under the action of many local factors, resulting in leakage [8,59,60].

In this experiment, we injected a contrast agent into the blood vessels of mice for angiography. As the blood circulating, the contrast agent enters the fundus of new blood vessels but leaks due to the fragility of the new blood vessels and forms a very bright circular image. The brightness of this circular image is positively correlated with the extent of CNV lesions in the area. as shown in Fig. 4C, the T-155 treatment significantly inhibited laser-induced choroidal leakage. Angiograms were graded using a leakage scoring system [54]. As shown in Table 3, the leakage score of the T-155 group was significantly lower than the other groups.

At the same time, we spread the choroidal tissues by using the method described above and stained them with isolectin B4 (IB4) to further confirm the efficacy of T-155 [43]. CNV lesions are identified by the location of the IB4 signal and fluorescence intensity. In contrast to angiography, isolectin binds to glycocalyx sugar residues in blood vessels, accurately labeling vascular endothelial cells without inducing blood vessel leakage and more intuitively showing the formation of new

blood vessels [61,62].

As shown in Fig. 4D, the large central fluorophore displayed nonspecific staining of the optic disc after the optic disc was peeled off. The neovascular area surrounds the optic disc in the CNV model. We focused on the local neovascularization area and obtained the high-magnification image (Fig. 4E). The neovascularization area was significantly reduced in the T-155 group. We used ImageJ software to perform a statistical analysis of the fluorescent area in each group. The fluorescent area of the T-155 group was significantly smaller than that in other groups.

3.7. T-155 reduces CNV by acting on macrophages to polarize them to the M1 type

We quantitated the length and area of the focal CNV lesions, and found that T-155 significantly attenuated CNV lesions in the laser-induced mouse model. We stained sections with the antibody against IBA-1, a marker of macrophages, and found macrophages were mainly distributed in the inner plexiform layer (IPL) and outer plexiform layer (OPL) of normal C57 mice. In the mouse CNV model, macrophages were activated and involved in the formation of new blood vessels. (supplementary data S6, S7) Macrophages were activated and invaded the focal CNV lesions in the T-155 group, as evidenced by immunohistochemical staining. Iba-1 was used as a general marker of macrophages. In the focal CNV lesion a large number of Iba-1+ macrophages could be found, while Iba-1+ macrophages were hardly detected in retinal sections from normal mice.

The effect of T-155 on CNV was examined using HE staining (Fig. 5A). The length and area of CNV lesions in the CRTL, tFNA, 155mimic and T-155 groups are shown in high-magnification images. Quantification of the length (***P < 0.001) and area (***P < 0.001) of CNV lesions is presented in histograms in Fig. 5B.

To further determine that the therapeutic effect of T-155 is related to macrophages polarization, we test some markers of macrophages polarization. According to the previous article, we also lay out the extracted eyeballs. We firstly locate the leakage area by staining the tissues with DAPI and IB4, and then stain the leakage area for markers of macrophages polarization. It can be seen that CD86, a marker of M1 type macrophages, was increased in the T-155 group. The expression of CD206, a marker of M2 type macrophages, was decreased (Fig. 5C and D).

Therefore, we inferred that T-155 improved CNV by activating macrophages and reducing VEGF secretion.

4. Conclusion

In this experiment, unlike other existing drugs on the market, we did not directly use VEGF as a target for the treatment of CNV, but explored the reasons for the abnormal increase of VEGF in CNV diseases, and used macrophages as our target. We found that after T-155 enters the cell, it can polarize macrophages into M1 type. Then we cocultured treated macrophages with human umbilical vein endothelial cells (HUVECs) to observe angiogenesis and found that macrophages treated with T-155 significantly inhibited HUVEC angiogenesis. Next, we used a laser to damage the mouse Bruch's membrane and obtain a mouse CNV model. On the fifth day after model establishment, the degree of CNV recovery in the mouse was judged by contrast injection and choroidal tissue mounts after vitreous administration. CNV was effectively controlled in mice injected with T-155. Thus, we further determined whether the effect of T-155 was mediated by macrophages. We performed immunohistochemical staining with an IBA1 antibody, a marker of macrophages, and found that the laser-damaged area contained aggregated macrophages, as evidenced by immunofluorescence staining. After the T-155 injection, the expression of VEGF decreased but the expression of iNOS, a marker of M1 cells, increased, which proved that T-155 improved CNV pathology by polarizing macrophages. CNV is a
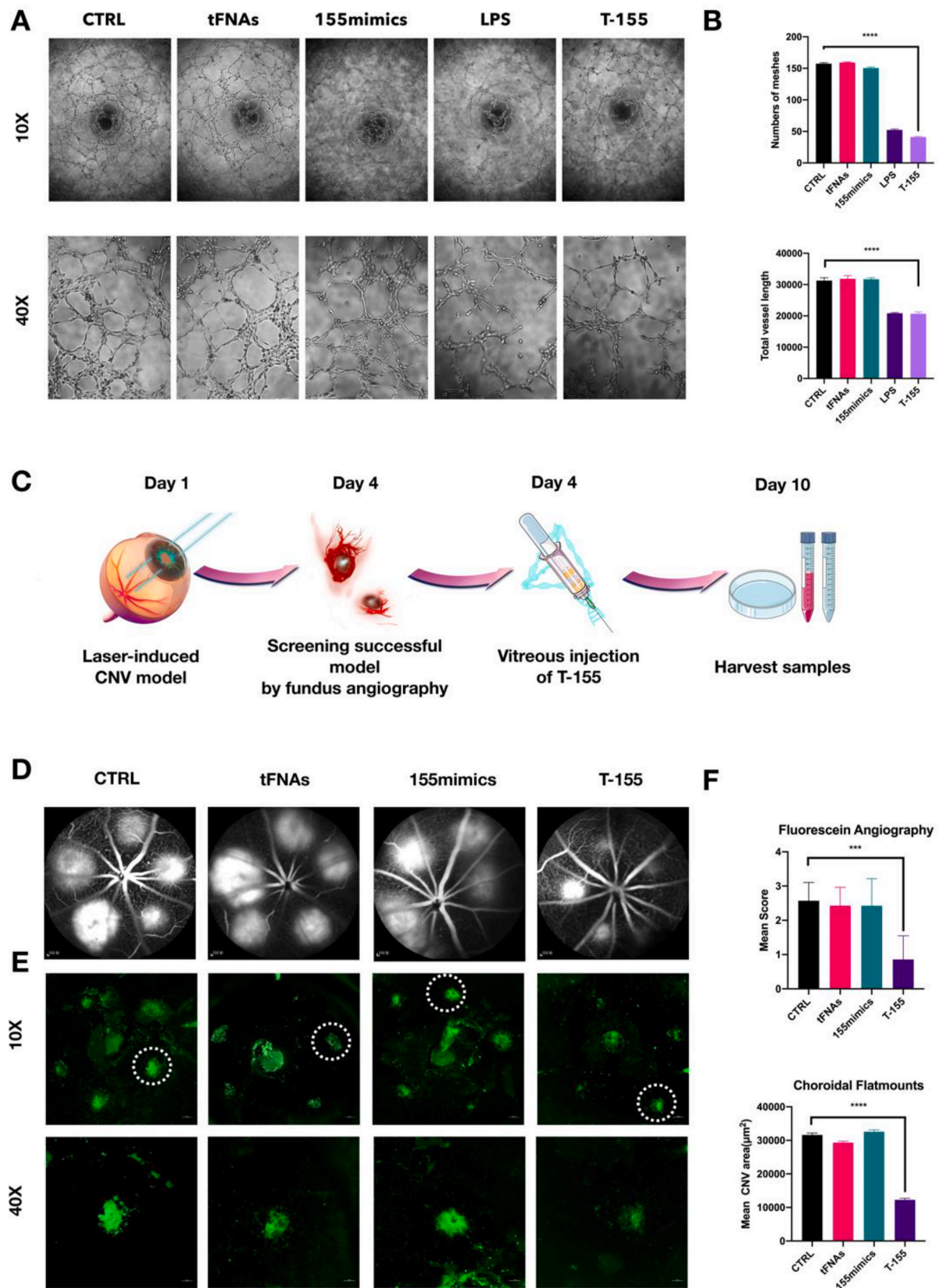
Fig. 4. T-155 treated macrophages inhibit angiogenesis *in vitro* and improve CNV lesions in vivo. (A) The results of angiogenesis experiments after co-cultured human umbilical vein endothelial cells (HUVECs)and macrophages which are after different treatments. (B) Analysis of the number and length of blood vessels. Data are presented as mean ± SD (n = 3). (C) Brief description of the in vivo experiment process. (D) Angiograms results of different groups. (E)The results of IB4 staining. (F) Score of CNV damage and statistics of leakage area. Data are presented as mean ± SD (n = 3). Statistical analysis: the ANOVA test was applied, ***p < 0.001 and ****p < 0.0001. All images in Figure are representative images.

Table 3
The leakage scores.

Signs	Score
No staining, faint hyperfluorescence	0
Staining	1
Moderate staining	2
Strong staining	3

pathological process that occurs widely in many diseases and the primary cause of blindness in the elderly. CNV mainly refers to the proliferating blood vessels of choroidal capillaries, but the pathogenesis of CNV has not yet been completely elucidated.

An increasing number of studies have shown that the formation of CNV is closely related to the dynamic balance of inflammation [8,18, 63]. In the process of CNV formation, various types of damage or stimuli cause choroidal inflammation and activate macrophages [64,65]. However, in the process of tissue repair, the excessive repair caused by the activation of macrophages produces excess VEGF, which might promote the formation of CNV [53]. Therefore, strategies regulating the

dynamic balance of the inflammatory response and repair response in the immune process have become a potential treatment for CNV.

MiRNA-155 is a miRNA that is quite active in the immune system and inflammatory response. According to previous studies, miRNA-155 regulates the inflammatory response towards the proinflammatory response and slows the repair response mediated by macrophages, thereby reducing the production of VEGF [66]. miR-155 inhibited M2 polarization through targeting C/EBPβ, suppressed VEGF expression and the formation of CNV after injury [43].

In addition to the innovative use of the macrophages as the target for the treatment of CNV, our RNA transfection system also uses tFNAs as the transport carrier. Compared with lipids and lentiviral transfection, this nanomaterial has superior biological safety in vivo. At the same time, studies have proven that tFNAs have good anti-inflammatory activity and promote cell proliferation and differentiation, laying a good foundation for these materials to carry miRNA-155 into cells to exert its effects [45,48]. In addition, we designed an elongated RNA sequence for the microRNA in this study that is complementary to the sequence extending from the top of tFNAs, achieving the self-assembly of miRNA and tFNAs, substantially improving the efficiency of synthesis and
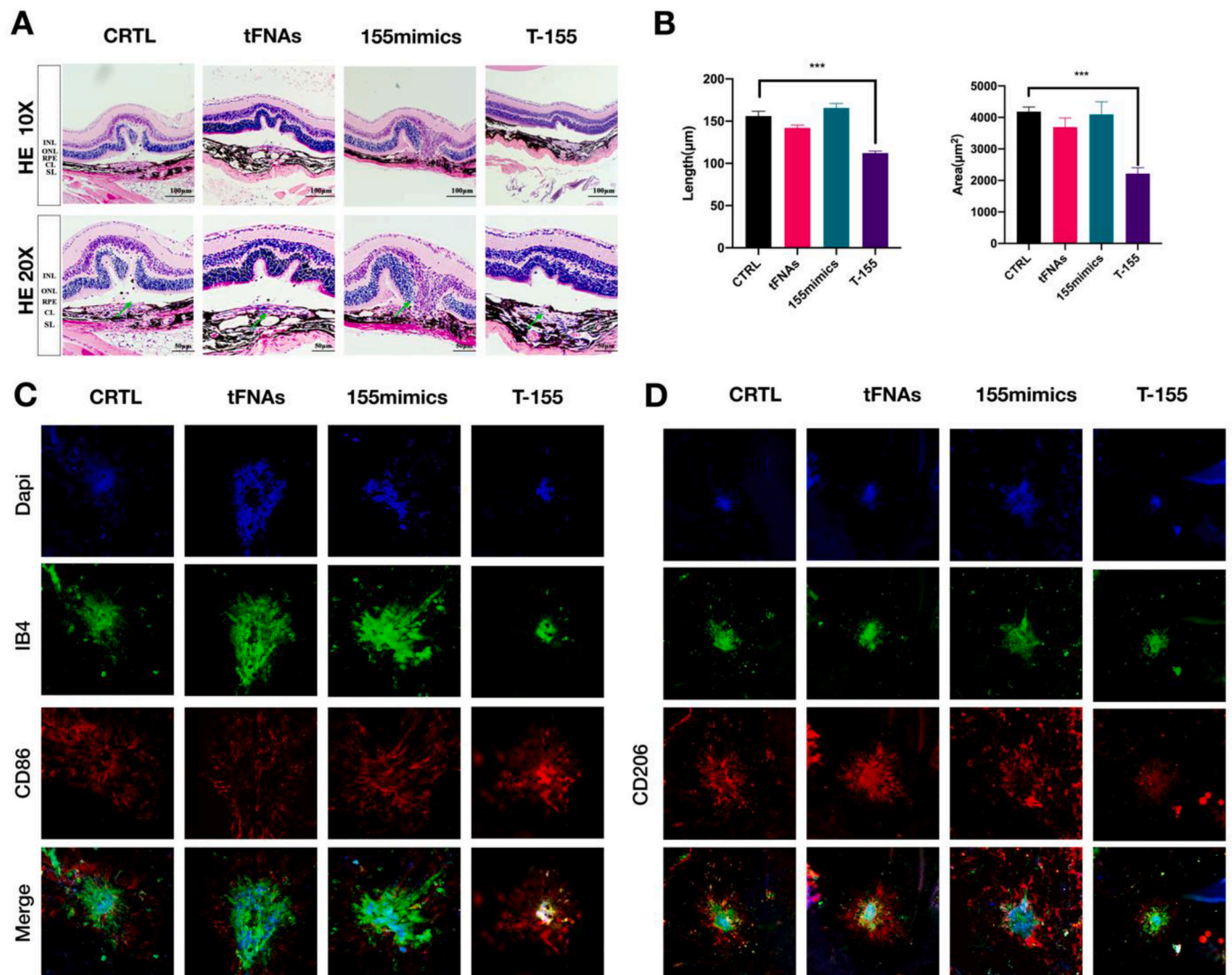

Fig. 5. T-155 promotes the polarization of macrophages in the injured area to M1 type and reduces CNV damage. (A) The results of HE staining in different groups. (B) Analysis of the area and length of CNV leakage. Data are presented as mean ± SD (n = 3) Statistical analysis: the ANOVA test was applied, ***p < 0.001 and ****p < 0.0001. (C) Immunofluorescence micrographs of VEGF (nucleus: blue, VEGF: red). Scale bars are 200 μm. (D) Immunofluorescence micrographs of iNOS (nucleus: blue, iNOS:green) (E)The results of immunostained choroidal flat mounts. (IB4: green, nucleus: blue, CD86: red) Scale bars are 50 μm, the same below (F) The results of immunostained choroidal flat mounts. (IB4: green, nucleus: blue, CD206: red) All images in Figure are representative images.

reducing the cost of synthesis [67].

In this experiment, we used various methods (such as PAGE, DLS, etc.) to verify the successful synthesis of tFNAs and T-155. Afterwards, we verified that tFNAs carrying miRNA-155 successfully entered the cell and bound to the target gene CEBP/β to reduce its expression. Therefore, we proved that tFNAs can be used as an excellent carrier to carry miRNA into cells, and that miRNA-155 can promote the polarization of macrophages, and it may play a part in the treatment of CNV.

Above all, we proved that macrophages accumulate in large numbers in the damaged area of CNV model, and promoting the polarization of these macrophages to M1 type can effectively improve the symptoms of CNV. At the same time, tFNAs is an effective RNA transport system.

In the future, we hope to further explore the relationship between macrophage polarization and CNV, the dynamic changes of macrophage polarization in the course of CNV disease, and the specific mechanisms by which macrophages function. At the same time, tFNAs carrying RNA is also an interesting attempt. Due to the special structure of tFNAs, RNA-linked T-155 still has the potential for modification. In the next experiment, targeted drugs or sustained-release systems can be connected to the remaining three vertices of T-155, which is expected to further solve the bottleneck of monotherapy and unsatisfactory long-term efficacy of existing drugs.

CRediT authorship contribution statement

Xin Qin: Conceptualization, Investigation, Methodology, Project administration, Writing – original draft. **Lirong Xiao:** Data curation, Formal analysis, Investigation, Writing – review & editing. **Ni Li:** Methodology, Investigation, Software. **Chen Hou:** Data curation, Methodology, Resources. **Wenman Li:** Data curation, Investigation, Writing – review & editing. **Jiajie Li:** Data curation, Methodology, Software. **Naihong Yan:** Resources, Methodology, Writing – review & editing. **Yunfeng Lin:** Project administration, Funding acquisition, Supervision, Writing – review & editing.

Declaration of competing interest

There are no conflicts of interest to declare.

Acknowledgements

Appendix A. Supplementary data

Supplementary data to this article can be found online at https://doi.org/10.1016/j.bioactmat.2021.11.031.

References

[1] L.S. Lim, P. Mitchell, J.M. Seddon, F.G. Holz, T.Y. Wong, Age-related macular degeneration, Lancet 379 (2012) 1728–1738, https://doi.org/10.1016/S0140-6736(12)60282-7.

[2] W.L. Wong, X. Su, X. Li, C.M.G. Cheung, R. Klein, C.Y. Cheng, T.Y. Wong, Global prevalence of age-related macular degeneration and disease burden projection for 2020 and 2040: a systematic review and meta-analysis, Lancet Global Health 2 (2014) e106–e116, https://doi.org/10.1016/S2214-109X(13)70145-1.

[3] D.S. Friedman, B.J. O'Colmain, B. Muñoz, S.C. Tomany, C. McCarty, P.T.V. M. DeJong, B. Nemesure, P. Mitchell, J. Kempen, N. Congdon, Prevalence of age-related macular degeneration in the United States, Arch. Ophthalmol. 122 (2004) 564–572, https://doi.org/10.1001/ARCHOPHT.122.4.564.

[4] L.F. Hernández-Zimbrón, R. Zamora-Alvarado, L. Ochoa-De La Paz, R. Velez-Montoya, E. Zenteno, R. Gulias-Cañizo, H. Quiroz-Mercado, R. Gonzalez-Salinas, Age-related macular degeneration: new paradigms for treatment and management of AMD, Oxid. Med. Cell. Longev. (2018), e8374647, https://doi.org/10.1155/2018/8374647, 2018.

[5] A.J. Augustin, J. Kirchhof, Inflammation and the pathogenesis of age-related macular degeneration, Expert Opin. Ther. Pat. 13 (2009) 641–651, https://doi.org/10.1517/14728220902942322.

[6] Y. Yang, F. Liu, M. Tang, M. Yuan, A. Hu, Z. Zhan, Z. Li, J. Li, X. Ding, L. Lu, Macrophage polarization in experimental and clinical choroidal neovascularization, Sci. Rep. 6 (2016), e30933, https://doi.org/10.1038/srep30933.

[7] S. Alivernini, E. Gremese, C. McSharry, B. Tolusso, G. Ferraccioli, I.B. McInnes, M. Kurowska-Stolarska, MicroRNA-155-at the critical interface of innate and adaptive immunity in arthritis, Front. Immunol. 8 (2018), e1932, https://doi.org/10.3389/FIMMU.2017.01932.

[8] H.E. Grossniklaus, J.X. Ling, T.M. Wallace, S. Dithmar, D.H. Lawson, C. Cohen, V. M. Elner, S.G. Elner, P. Sternberg Jr., Macrophage and retinal pigment epithelium expression of angiogenic cytokines in choroidal neovascularization, Mol. Vis. 8 (2002) 119–126.

[9] P.S. Mettu, M.J. Allingham, S.W. Cousins, Incomplete response to Anti-VEGF therapy in neovascular AMD: exploring disease mechanisms and therapeutic opportunities, Prog. Retin. Eye Res. 82 (2021), https://doi.org/10.1016/j.preteyeres.2020.100906, 100906-100906.

[10] A. Caicedo, D.G. Espinosa-Heidmann, Y. Piña, E.P. Hernandez, S.W. Cousins, Blood-derived macrophages infiltrate the retina and activate Muller glial cells under experimental choroidal neovascularization, Exp. Eye Res. 81 (2005) 38–47, https://doi.org/10.1016/J.EXER.2005.01.013.

[11] S. Droho, B.R. Thomson, H.M. Makinde, C.M. Cuda, H. Perlman, J.A. Lavine, Ocular macrophage origin and heterogeneity during steady state and experimental choroidal neovascularization, J. Neuroinflammation 17 (2020) e341, https://doi.org/10.1186/S12974-020-02010-0.

[12] A. Sica, A. Mantovani, Macrophage plasticity and polarization: in vivo veritas, J. Clin. Invest. 122 (2012) 787–795, https://doi.org/10.1172/JCI59643.

[13] B. Martinez, P.V. Peplow, MicroRNAs in laser-induced choroidal neovascularization in mice and rats: their expression and potential therapeutic targets, Neur. Regener. Res. 16 (2021) 621.

[14] S. Gordon, F.O. Martinez, Alternative activation of macrophages: mechanism and functions, Immunity 32 (2010) 593–604, https://doi.org/10.1016/J.IMMUNI.2010.05.007.

[15] L. Parisi, E. Gini, D. Baci, M. Tremolati, M. Fanuli, B. Bassani, G. Farronato, A. Bruno, L. Mortara, Macrophage polarization in chronic inflammatory diseases: killers or builders? J. Immunol. Res. 2018 (2018), e8917804 https://doi.org/10.1155/2018/8917804.

[16] J. Liu, D.A. Copland, S. Horie, W.K. Wu, M. Chen, Y. Xu, B. Paul Morgan, M. Mack, H. Xu, L.B. Nicholson, A.D. Dick, Myeloid cells expressing VEGF and arginase-1 following uptake of damaged retinal pigment epithelium suggests potential mechanism that drives the onset of choroidal angiogenesis in mice, PLoS One 8 (2013), e72935, https://doi.org/10.1371/JOURNAL.PONE.0072935.

[17] L. He, A.G. Marneros, Macrophages are essential for the early wound healing response and the formation of a fibrovascular scar, Am. J. Pathol. 182 (2013) 2407–2417, https://doi.org/10.1016/j.ajpath.2013.02.032.

[18] S. Brandenburg, A. Müller, K. Turkowski, Y.T. Radev, S. Rot, C. Schmidt, A. D. Bungert, G. Acker, A. Schorr, A. Hippe, K. Miller, F.L. Heppner, B. Homey, P. Vajkoczy, Resident microglia rather than peripheral macrophages promote vascularization in brain tumors and are source of alternative pro-angiogenic factors, Acta Neuropathol. 131 (2016) 365–378, https://doi.org/10.1007/S00401-015-1529-6.

[19] C.T. Supuran, Agents for the prevention and treatment of age-related macular degeneration and macular edema: a literature and patent review, Expert Opin. Ther. Pat. 29 (2019) 761–767, https://doi.org/10.1080/13543776.2019.1671353.

[20] D. Ardeljan, C.C. Chan, Aging is not a disease: distinguishing age-related macular degeneration from aging, Prog. Retin. Eye Res. 37 (2013) 68–89, https://doi.org/10.1016/J.PRETEYERES.2013.07.003.

[21] M. Suzuki, N. Nagai, K. Izumi-Nagai, H. Shinoda, T. Koto, A. Uchida, H. Mochimaru, K. Yuki, M. Sasaki, K. Tsubota, Y. Ozawa, Predictive factors for non-response to intravitreal ranibizumab treatment in age-related macular degeneration, Br. J. Ophthalmol. 98 (2014) 1186–1191, https://doi.org/10.1136/BJOPHTHALMOL-2013-304670.

[22] S. Yang, J. Zhao, X. Sun, Resistance to anti-VEGF therapy in neovascular age-related macular degeneration: a comprehensive review, Drug Des. Dev. Ther. 10 (2016) 1857–1867, https://doi.org/10.2147/DDDT.S97653.

[23] W. Cui, X. Yang, X. Chen, D. Xiao, J. Zhu, M. Zhang, X. Qin, X. Ma, Y. Lin, Treating LRRK2-related Parkinson's disease by inhibiting the mTOR signaling pathway to restore autophagy, Adv. Funct. Mater. (2021) 2105152.

[24] J. Li, L. Xiao, N. Yan, Y. Li, Y. Wang, X. Qin, D. Zhao, M. Liu, N. Li, Y. Lin, The neuroprotective effect of MicroRNA-22-3p modified tetrahedral framework nucleic acids on damaged retinal neurons via TrkB/BDNF signaling pathway, Adv. Funct. Mater. 31 (2021) 2104141.

[25] W. Fu, L. Ma, Y. Ju, J. Xu, H. Li, S. Shi, T. Zhang, R. Zhou, J. Zhu, R. Xu, Therapeutic siCCR2 loaded by tetrahedral framework DNA nanorobotics in therapy for intracranial hemorrhage, Adv. Funct. Mater. (2021) 2101435.

[26] T. Tian, D. Xiao, T. Zhang, Y. Li, S. Shi, W. Zhong, P. Gong, Z. Liu, Q. Li, Y. Lin, A framework nucleic acid based robotic nanobee for active targeting therapy, Adv. Funct. Mater. 31 (2021) 2007342.

[27] Y. Li, S. Gao, S. Shi, D. Xiao, S. Peng, Y. Gao, Y. Zhu, Y. Lin, Tetrahedral framework nucleic acid-based delivery of resveratrol alleviates insulin resistance: from innate to adaptive immunity, Nano-Micro Lett. 13 (2021) 1–16.

[28] S. Gao, Y. Li, D. Xiao, M. Zhou, X. Cai, Y. Lin, Tetrahedral framework nucleic acids induce immune tolerance and prevent the onset of type 1 diabetes, Nano Lett. 21 (2021) 4437–4446.

[29] Q. Zhang, S. Lin, L. Wang, S. Peng, T. Tian, S. Li, J. Xiao, Y. Lin, Tetrahedral framework nucleic acids act as antioxidants in acute kidney injury treatment, Chem. Eng. J. 413 (2021) 127426.

[30] Y. Sun, Y. Liu, B. Zhang, S. Shi, T. Zhang, D. Zhao, T. Tian, Q. Li, Y. Lin, Erythromycin loaded by tetrahedral framework nucleic acids are more antimicrobial sensitive against Escherichia coli (E. coli), Bioact. Mater. 6 (2021) 2281–2290.

[31] M. Zhou, S. Gao, X. Zhang, T. Zhang, T. Zhang, T. Tian, S. Li, Y. Lin, X. Cai, The protective effect of tetrahedral framework nucleic acids on periodontium under inflammatory conditions, Bioact. Mater. 6 (2021) 1676–1688.

[32] L. Meng, W. Ma, M. Zhang, R. Zhou, Q. Li, Y. Sun, W. Fu, X. Cai, Y. Lin, Aptamer-guided DNA tetrahedrons as a photo-responsive drug delivery system for Mucin 1-expressing breast cancer cells, Appl. Mater. Today 23 (2021) 101010.

[33] T. Zhang, T. Tian, R. Zhou, S. Li, W. Ma, Y. Zhang, N. Liu, S. Shi, Q. Li, X. Xie, Design, fabrication and applications of tetrahedral framework nucleic acid-based multifunctional complexes in drug delivery and biomedical treatment, Nat. Protoc. 15 (2020) 2728–2757.

[34] J. Zhu, M. Zhang, Y. Gao, X. Qin, T. Zhang, W. Cui, C. Mao, D. Xiao, Y. Lin, Tetrahedral framework nucleic acids promote scarless healing of cutaneous wounds via the AKT-signaling pathway, Signal Transd. Target. Thera. 5 (2020) 1–11.

[35] Y. Zhang, X. Xie, W. Ma, Y. Zhan, C. Mao, X. Shao, Y. Lin, Multi-targeted antisense oligonucleotide delivery by a framework nucleic acid for inhibiting biofilm formation and virulence, Nano-Micro Lett. 12 (2020) 1–13.

[36] Y. Liu, Y. Sun, S. Li, M. Liu, X. Qin, X. Chen, Y. Lin, Tetrahedral framework nucleic acids deliver antimicrobial peptides with improved effects and less susceptibility to bacterial degradation, Nano Lett. 20 (2020) 3602–3610.

[37] S. Sirong, C. Yang, T. Taoran, L. Songhang, L. Shiyu, Z. Yuxin, S. Xiaoru, Z. Tao, L. Yunfeng, C. Xiaoxiao, Effects of tetrahedral framework nucleic acid/wogonin complexes on osteoarthritis, Bone Res. 8 (2020) 1–13.

[38] M. Zhang, X. Zhang, T. Tian, Q. Zhang, Y. Wen, J. Zhu, D. Xiao, W. Cui, Y. Lin, Anti-inflammatory activity of curcumin-loaded tetrahedral framework nucleic acids on acute gouty arthritis, Bioact. Mater. 8 (2022) 368–380.

[39] G. Mahesh, R. Biswas, MicroRNA-155: a master regulator of inflammation, J. Interferon Cytokine Res. 39 (2019) 321–330, https://doi.org/10.1089/JIR.2018.0155.

[40] E.D. Ponomarev, T. Veremeyko, H.L. Weiner, MicroRNAs are universal regulators of differentiation, activation, and polarization of microglia and macrophages in normal and diseased CNS, Glia 61 (2013) 91–103, https://doi.org/10.1002/GLIA.22363.

[41] T.S. Elton, H. Selemon, S.M. Elton, N.L. Parinandi, Regulation of the MIR155 host gene in physiological and pathological processes, Gene 532 (2013) 1–12, https://doi.org/10.1016/J.GENE.2012.12.009.

[42] Y. Zhu, W. Tan, A.M. Demetriades, Y. Cai, Y. Gao, A. Sui, Q. Lu, X. Shen, C. Jiang, B. Xie, X. Sun, Interleukin-17A neutralization alleviated ocular neovascularization by promoting M2 and mitigating M1 macrophage polarization, Immunology 147 (2016) 414–428, https://doi.org/10.1111/IMM.12571.

[43] P. Zhang, H. Wang, X. Luo, H. Liu, B. Lu, T. Li, S. Yang, Q. Gu, B. Li, F. Wang, X. Sun, MicroRNA-155 inhibits polarization of macrophages to M2-type and suppresses choroidal neovascularization, Inflammation 41 (2018) 143–153, https://doi.org/10.1007/S10753-017-0672-8.

[44] B. Martinez, P.V. Peplow, MicroRNAs in laser-induced choroidal neovascularization in mice and rats: their expression and potential therapeutic targets, Neural Regen. Res. 16 (2021) 621–627, https://doi.org/10.4103/1673-5374.295271.

[45] J. Zhu, M. Zhang, Y. Gao, X. Qin, T. Zhang, W. Cui, C. Mao, D. Xiao, Y. Lin, Tetrahedral framework nucleic acids promote scarless healing of cutaneous wounds via the AKT-signaling pathway, Signal Transduct. Target. Ther. 5 (2020) 1–11, https://doi.org/10.1038/s41392-020-0173-3.

[46] Q. Zhang, S. Lin, S. Shi, T. Zhang, Q. Ma, T. Tian, T. Zhou, X. Cai, Y. Lin, Anti-inflammatory and antioxidative effects of tetrahedral DNA nanostructures via the modulation of macrophage responses, ACS Appl. Mater. Interfaces 10 (2018) 3421–3430, https://doi.org/10.1021/ACSAMI.7B17928.

[47] S. Li, T. Tian, T. Zhang, X. Cai, Y. Lin, Advances in biological applications of self-assembled DNA tetrahedral nanostructures, Mater, Today Off. 24 (2019) 57–68, https://doi.org/10.1016/J.MATTOD.2018.08.002.

[48] X. Qin, N. Li, M. Zhang, S. Lin, J. Zhu, D. Xiao, W. Cui, T. Zhang, Y. Lin, X.X. Cai, Tetrahedral framework nucleic acids prevent retina ischemia-reperfusion injury from oxidative stress: via activating the Akt/Nrf2 pathway, Nanoscale 11 (2019) 20667–20675, https://doi.org/10.1039/C9NR07171G.

[49] W. Fu, C. You, L. Ma, H. Li, Y. Ju, X. Guo, S. Shi, T. Zhang, R. Zhou, Y. Lin, Enhanced efficacy of temozolomide loaded by a tetrahedral framework DNA nanoparticle in the therapy for glioblastoma, ACS Appl. Mater. Interfaces 11 (2019) 39525–39533, https://doi.org/10.1021/ACSAMI.9B13829.

[50] Y. Fujio, T. Nguyen, D. Wencker, R.N. Kitsis, K. Walsh, Akt promotes survival of cardiomyocytes in vitro and protects against lschemia-reperfusion injury in mouse heart, Circulation 101 (2000) 660–667, https://doi.org/10.1161/01.CIR.101.6.660.

[51] L. Cao, H. Wang, F. Wang, D. Xu, F. Liu, C. Liu, Aβ-induced senescent retinal pigment epithelial cells create a proinflammatory microenvironment in AMD, Investig. Ophthalmol. Vis. Sci. 54 (2013) 3738–3750, https://doi.org/10.1167/iovs.13-11612.

[52] Q. Li, D. Zhao, X. Shao, S. Lin, X. Xie, M. Liu, W. Ma, S. Shi, Y. Lin, Aptamer-modified tetrahedral DNA nanostructure for tumor-targeted drug delivery, ACS Appl. Mater. Interfaces 9 (2017) 36695–36701, https://doi.org/10.1021/ACSAMI.7B13328.

[53] L. He, A.G. Marneros, Doxycycline inhibits polarization of macrophages to the proangiogenic M2-type and subsequent neovascularization, J. Biol. Chem. 289 (2014) 8019–8028, https://doi.org/10.1074/JBC.M113.535765.

[54] W. Zhang, L. Dai, X. Li, Y. Li, M.K. Hung Yap, L. Liu, H. Deng, SARI prevents ocular angiogenesis and inflammation in mice, J. Cell Mol. Med. 24 (2020) 4341–4349.

[55] F. Parmeggiani, C. Campa, C. Costagliola, C. Incorvaia, C. Sheridan, F. Semeraro, K. De Nadai, A. Sebastiani, Inflammatory mediators and angiogenic factors in choroidal neovascularization: pathogenetic interactions and therapeutic implications, Mediat. Inflamm. 2010 (2010), e546826, https://doi.org/10.1155/2010/546826.

[56] N. Nagai, P.L. von Leithner, K. Izumi-Nagai, B. Hosking, B. Chang, R. Hurd, P. Adamson, A.P. Adamis, R.H. Foxton, Y.S. Ng, D.T. Shima, Spontaneous CNV in a novel mutant mouse is associated with early VEGF-A-driven angiogenesis and late-stage focal edema, neural cell loss, and dysfunction, Investig. Ophthalmol. Vis. Sci. 55 (2014) 3709–3719, https://doi.org/10.1167/IOVS.14-13989.

[57] J.Z. Nowak, Age-related macular degeneration (AMD): pathogenesis and therapy, Pharmacol. Rep. 58 (2006) 353–363.

[58] A.V. Chappelow, K. Tan, N.K. Waheed, P.K. Kaiser, Panretinal photocoagulation for proliferative diabetic retinopathy: pattern scan laser versus argon laser, Am. J. Ophthalmol. 153 (2012) 137–142, https://doi.org/10.1016/J.AJO.2011.05.035, e132.

[59] C.N. Nagineni, V.K. Kommineni, A. William, B. Detrick, J.J. Hooks, Regulation of VEGF expression in human retinal cells by cytokines: implications for the role of inflammation in age-related macular degeneration, J. Cell. Physiol. 227 (2012) 116–126, https://doi.org/10.1002/JCP.22708.

[60] V. Lambert, J. Lecomte, S. Hansen, S. Blacher, M.L.A. Gonzalez, I. Struman, N. E. Sounni, E. Rozet, P. De Tullio, J.M. Foidart, J.M. Rakic, A. Noel, Laser-induced choroidal neovascularization model to study age-related macular degeneration in mice, Nat. Protoc. 8 (2013) 2197–2211, https://doi.org/10.1038/NPROT.2013.135.

[61] M. Campos, J. Amaral, S.P. Becerra, R.N. Fariss, A novel imaging technique for experimental choroidal neovascularization, Investig. Ophthalmol. Vis. Sci. 47 (2006) 5163–5170, https://doi.org/10.1167/iovs.06-0156.

[62] I. Fukushima, K. Kusaka, K. Takahashi, N. Kishimoto, T. Nishimura, H. Ohkuma, M. Uyama, Comparison of indocyanine green and fluorescein angiography of choroidal neovascularization, Jpn. J. Ophthalmol. 41 (1997) 284–296, https://doi.org/10.1016/S0021-5155(97)00058-0.

[63] Y. Xu, K. Cui, J. Li, K. Tang, J. Lin, X. Lu, R. Huang, B. Yang, Y. Shi, D. Ye, J. Huang, S. Yu, X. Liang, Melatonin attenuates choroidal neovascularization by regulating macrophage/microglia polarization via inhibition of RhoA/ROCK signaling pathway, J. Pineal Res. 69 (2020), e12660, https://doi.org/10.1111/JPI.12660.

[64] C. Tsutsumi, K.-H. Sonoda, K. Egashira, H. Qiao, T. Hisatomi, S. Nakao, M. Ishibashi, I.F. Charo, T. Sakamoto, T. Murata, T. Ishibashi, The critical role of ocular-infiltrating macrophages in the development of choroidal neovascularization, J. Leukoc. Biol. 74 (2003) 25–32, https://doi.org/10.1189/JLB.0902436.

[65] X. Peng, H. Xiao, M. Tang, Z. Zhan, Y. Yang, L. Sun, X. Luo, A. Zhang, X. Ding, Mechanism of fibrosis inhibition in laser induced choroidal neovascularization by doxycycline, Exp. Eye Res. 176 (2018) 88–97, https://doi.org/10.1016/J.EXER.2018.06.030.

[66] X. Wang, Y. Chen, W. Yuan, L. Yao, S. Wang, Z. Jia, P. Wu, L. Li, P. Wei, X. Wang, M. Hong, MicroRNA-155-5p is a key regulator of allergic inflammation, modulating the epithelial barrier by targeting PKIα, Cell Death Dis. 10 (2019) 1–14, https://doi.org/10.1038/S41419-019-2124-X.

[67] Y. Li, S. Gao, S. Shi, D. Xiao, S. Peng, Y. Gao, Y. Zhu, Y. Lin, Tetrahedral framework nucleic acid-based delivery of resveratrol alleviates insulin resistance: from innate to adaptive immunity, Nano-Micro Lett. 13 (2021), https://doi.org/10.1007/s40820-021-00614-6, 86-86.